Liquid Metal-Controlled Dual-Band Doppler Radar for Enhanced Velocity Measurement

Anıl Karatay; Fatih Yaman

Published version information

Citation: A. Karatay and F. Yaman, "Liquid Metal-Controlled Dual-Band Doppler Radar for Enhanced Velocity Measurement," in *IEEE Transactions on Instrumentation and Measurement*, vol. 73, pp. 1-8, 2024, Art no. 8001108

DOI: https://doi.org/10.1109/TIM.2023.3343776

Liquid Metal-Controlled Dual-Band Doppler Radar for Enhanced Velocity Measurement

Anıl Karatay and Fatih Yaman *

Abstract

Doppler radars, which are critical instruments for velocity measurement, may need to be reconfigured to adapt to different environmental conditions or for ease of use. However, conventional electrical, optical, and physical reconfiguration methods often come with several disadvantages such as deteriorated radiation pattern, reduced radiation efficiency and high cost. Therefore, the aim of this paper is to integrate microwave components that can be controlled using liquid metal (LM) displacement into a Doppler radar to adjust its main lobe direction and operating frequency to the desired values and enhance the measurement capacity of the respective radar. Through this study, multiple parameters of an operational Doppler radar have been simultaneously adjusted using LM displacement exploitation for the first time, thus avoiding the shortcomings associated with conventional reconfiguration methods. To achieve this objective, initially, a back-to-back Vivaldi antenna operating at 2.45 GHz is designed, and beam switching ability is imparted to the structure using the LM displacement method. Subsequently, various techniques are employed to convert the structure into a dual-band antenna capable of simultaneous operation at 2.45 GHz and 5.8 GHz, ensuring the desired beam switching feature at both frequencies. Additionally, a power divider capable of switching between the two operating frequencies through LM assistance is proposed, and its integration into the radar system enables the control of both main lobe direction and frequency using the proposed method.

radar, antenna, liquid metal, microstrip, gallium

1 Introduction

Given the dynamic nature of environmental conditions and the rapid advancement of technology, there arises a need to reconfigure the antennas or any other components within radar systems to maintain peak performance [1,2]. Depending on specific requirements, one can manipulate the electromagnetic characteristics of these components through diverse methods involving electrical, optical,

*The authors are with the Department of Electrical and Electronics Engineering, İzmir Institute of Technology, Urla, İzmir, 35430 Türkiye. F. Yaman is also with ASTeC, STFC Daresbury Laboratory, WA4 4AD Warrington, United Kingdom. e-mail: anilkaratay@iyte.edu.tr.

or physical alterations, as documented in the literature [3, 4]. However, each of these techniques presents its unique set of challenges and constraints. While electrical reconfiguration methods offer the advantage of high-speed switching [5], they can introduce disruptions to the antenna's radiation pattern and necessitate intricate integration processes, often involving components like PIN diodes and RF MEMS [6]. Moreover, achieving high radiation efficiency through electrical means is hindered by the discrete nature of PIN diodes [7]. Optical reconfiguration methods address the pattern degradation issue observed in electrical approaches but demand intricate integration of photoconductive materials and laser diodes, making them less attractive for cost-effective applications and resource-limited environments [8]. On the other hand, physical variations-based reconfiguration methods tend to suffer from slower switching speeds and complex integration procedures.

An alternative solution to these challenges is the LM-assisted reconfiguration method discussed in this paper. This method offers a reasonable switching rate for the appropriate application and provides benefits such as low loss, linear behavior, easy integration, and low cost [9]. Unlike electrically reconfigurable antennas, these structures are purely mechanical-based and demonstrate a highly linear behavior. There have been numerous studies on LM-assisted antenna technology including static antenna structures [10, 11], pattern reconfigurable [12–14], polarization reconfigurable [15, 16], frequency reconfigurable [17, 18], and bandwidth reconfigurable antennas [19]. However, these studies primarily focus on demonstrating the proof-of-concept for individual components rather than actively pursuing efforts to enhance the performance of a functioning system. Furthermore, due to the predominant focus of research on antennas, there exists a significant gap in the literature concerning the designs and LM-assisted reconfiguration of other microwave components. In this context, the concurrent design of different microwave components for simultaneous control via LM, their seamless integration into a radar system, and the consequent transformation of the radar into the LM displacement-controllable entity represents a novel endeavor not previously undertaken.

This study represents a pioneering effort by demonstrating the novel application of LM displacement to enhance the performance of an operating Doppler radar system. Firstly, a gallium-based technique was applied to a single-band Vivaldi antenna at 2.45 GHz, enabling the beam switching. Subsequently, this single-band antenna was transformed into a dual-band back-to-back Vivaldi antenna operating at 2.45 GHz and 5.8 GHz. The proposed design not only accomplishes beam switching via the displacement of LM but also mitigates issues such as pattern distortion, a prevalent concern in electrical methods, and the substantial cost barriers typically associated with optical techniques. Additionally, a novel power divider capable of frequency switching between 2.45 GHz and 5.8 GHz through LM displacement was proposed and integrated into the radar system. This integration allows the radar to seamlessly transition between frequencies and enhances its adaptability in the face of interference threats. These innovations collectively demonstrate the feasibility of LM-based reconfiguration in enhancing multiple parameters of an operational radar sys-

tem and, by extension, improving the performance of MIT Coffee Can Doppler Radar (MIT-CCDR) with continuous wave (CW) operations [20–22]. Such configurations are commonly utilized for short-range operations, primarily owing to their cost-effectiveness and easy deployability, rendering them a favored option [23, 24].

Materials with similar conductivity values and, importantly, non-toxic properties, such as EGaIn or Galinstan, can also be used for the same objective. For the specific purpose of maintaining the low-cost nature of the radar, pure gallium, a more cost-effective, more accessible and non-toxic material to touch, is utilized in this study. While its melting temperature is 29 °C, the proposed reconfiguration methods have been successfully demonstrated with this metal, which, once heated sufficiently, may take hours to return to a solid state. In addition to the advantages mentioned above, the LM-based radar exhibits a more durable operational performance due to its resistance to moisture and high temperatures and the absence of maintenance requirements compared to PIN diodes, which are susceptible to degradation. Furthermore, the proposed radar is considered cost-effective, thanks to the low quantity of LM used. In this context, the proposed radar can be utilized in resource-limited conditions, particularly where maintenance opportunities are scarce and spare parts may be in short supply. Being mechanically based, it is more resilient in high-humidity environments where electrical equipment like PIN diodes might be prone to damage.

2 LM-Assisted Single-Band Vivaldi Antenna at 2.45 GHz

This section is devoted to the applicability of LM-assisted beam switching to a single-band back-to-back Vivaldi antenna operating at 2.45 GHz.

2.1 Design of the LM-Assisted Single-Band Vivaldi Antenna

Using the displacement of ~ 1 g of gallium, that can be obtained at an exceptionally low cost owing to its limited quantity, the antenna achieves beam switching. For the dielectric layer of the antenna, an FR-4 substrate with 1.5 mm thickness, 4.3 dielectric constant, and 0.025 loss tangent was used. Since the primary purpose here is to use two Vivaldi antennas back-to-back, it is necessary to reduce the back-lobe level of the elements. We dug slots into the sides of the metal surface of the antenna to minimize the back-lobe level of the individual elements of the antenna array.

We considered a single-element Vivaldi antenna before forming the 2×1 Vivaldi antenna structure and conducting various investigations. The circular region with a diameter of d of a Vivaldi antenna given in Fig. 1 is critical for the antenna's radiation efficiency. According to the simulation results obtained

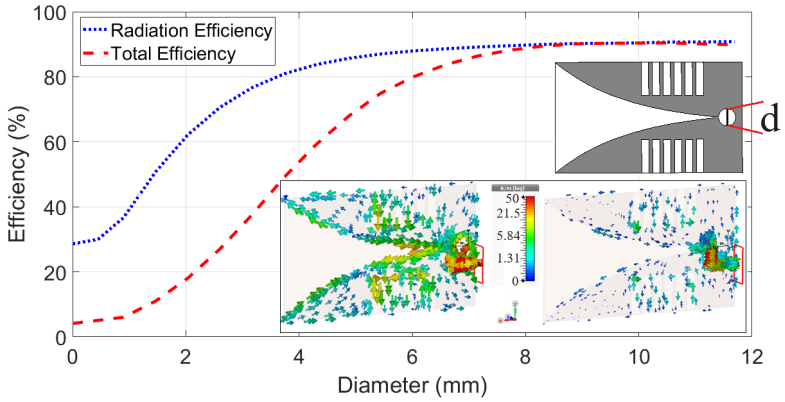

Figure 1: Radiation and total efficiency changes of a single-element Vivaldi antenna at 2.45 GHz w.r.t. the diameter of the cavity. The surface currents in the lower right correspond to $d = 9.7$ mm and completely filled cavity, respectively.

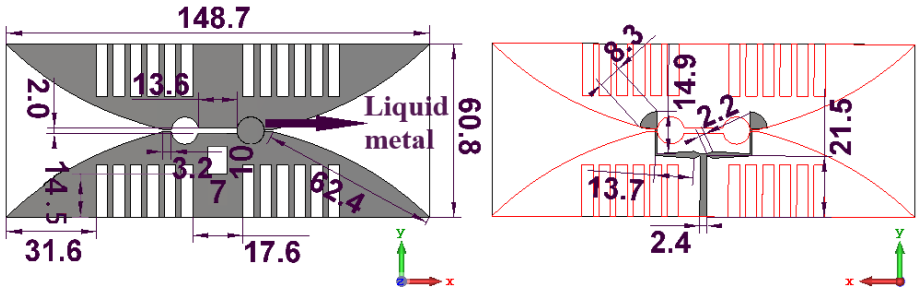

Figure 2: The dimensions of the single-band back-to-back Vivaldi antennas operating at 2.45 GHz (the dimensions are given in mm)

in Computer Simulation Technology - Microwave Studio (CST-MWS), the radiation efficiency of this antenna was found to be 90.3% at 2.45 GHz when $d = 9.7$ mm. If this region is completely filled with gallium, this value decreased to 28.6% in the simulation; see Fig. 1. Filling the cavity with LM may also disrupts the impedance matching, leading to a decrease in total efficiency to 4.2%. This will form the basis for designing two Vivaldi antennas back-to-back as the LM assisted beam switchable antenna.

After careful examination, a back-to-back Vivaldi antenna can be formed. The antenna's structure and the dimensions are given in Fig. 2. The input width of the feed line was optimized such that the input impedance was set to 50 Ω. To ensure impedance matching at the operating frequencies, a defected ground structure (DGS), whose dimensions are 10×7 mm^2 with 14.5 mm distance from the bottom edge, was placed behind the feedline, and the position and dimensions of this structure were determined parametrically through a detailed analysis. After placing the two antennas back-to-back employing a

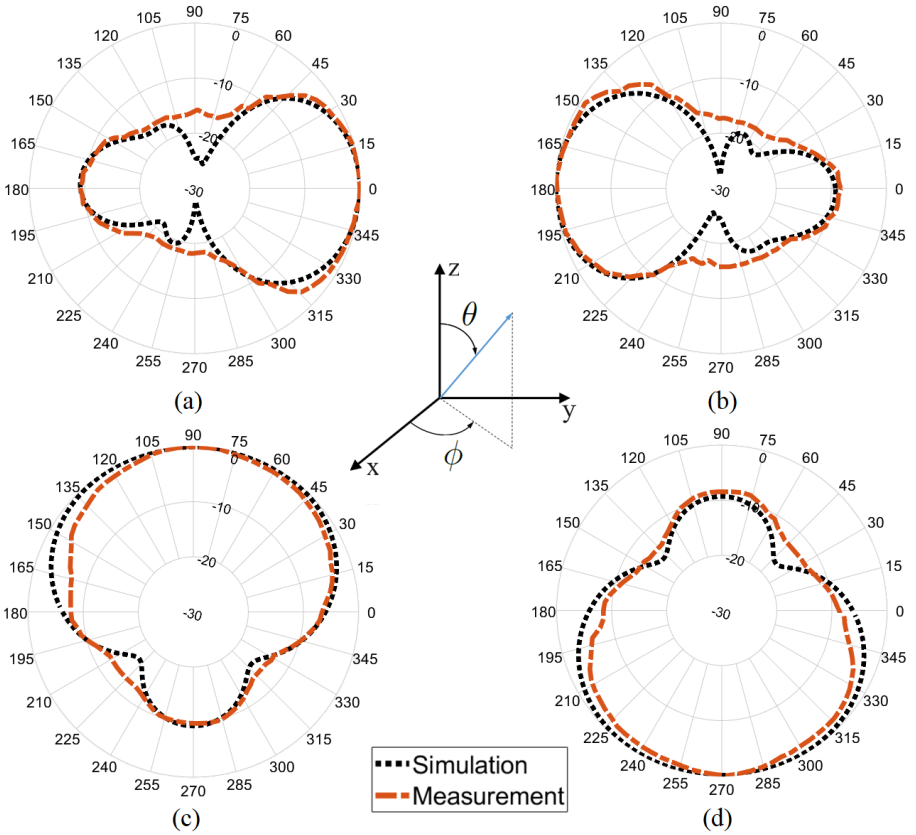

Figure 3: Normalized far-field plots of the single-band back-to-back Vivaldi antenna at 2.45 GHz (a) State-1 when $\theta = 90°$ (b) State-2 when $\theta = 90°$ (c) State-1 when $\phi = 0°$ (d) State-2 when $\phi = 0°$

divider, a fluidic line was placed between the circular cavities of the antenna. The primary purpose of the fluid line placed on the antenna is to ensure the flow of liquid gallium from one cavity to the other by tilting the antenna. The main lobe direction reaches its maximum value towards +x when the left cavity is filled with gallium (State-1), and towards the -x direction when the right cavity is filled (State-2).

2.2 Results of the LM-Assisted Single-Band Vivaldi Antenna

The antenna has been fabricated using the photolithography method, employing FR-4 material coated with a layer of photoresist. The liquid holder was produced with the help of a 3D printer to both preserve the shape of gallium and prevent any damage to copper, as gallium can interact with copper. The far-field plots,

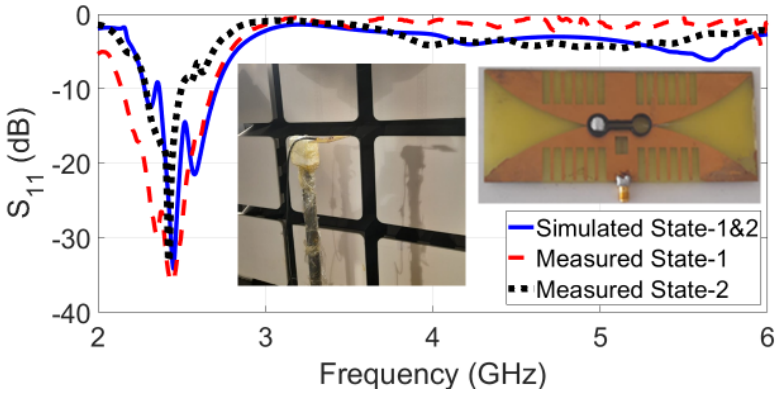

Figure 4: S-parameters of the single-band back-to-back Vivaldi antenna

fabricated prototype, and scattering parameters can be seen in Fig. 3 and Fig. 4. The maximum gain in the simulation was 5.11 dBi, and it was 4.76 dBi in the measurement. The simulated front-to-back ratio (FBR) for both states is 9.2 dB. In the measurement, the fact that the FBR values are 10.1 dB for State-1 and 9 dB for State-2 shows us that the measurements give close results with simulations. On the other hand, according to both measurement and simulation results, the antenna has a sufficiently low reflection coefficient at 2.45 GHz; see Fig. 4. Note that we used a thin tape with a low dielectric constant and 100 μm thickness to prevent gallium from flowing out when the antenna had to be turned sideways in the anechoic chamber measurements.

3 LM-Assisted Dual-Band Vivaldi Antenna

In the case of high power interference at 2.45 GHz, the radar is intended to switch its operating frequency to 5.8 GHz. Furthermore, it is desired for the antenna to possess the feature of LM-assisted beam switching at both operating frequencies.

3.1 Design of the LM-Assisted Dual-Band Vivaldi Antenna

The antenna's dielectric layer employs an FR-4 substrate with the same parameters given in the previous section. The dimensions of the Vivaldi antenna design are given in Fig. 5 in millimeters. The behavior has been simulated to ensure its validity at both working frequencies of the antenna. As shown in Fig. 6, the circular regions of the antenna are filled to obtain the desired radiation patterns. In this context, simulations were performed for 2.45 GHz and 5.8 GHz for State-1, by filling only the inside of the cavity with gallium as in Fig. 6-(a). The normalized far-field results for 2.45 GHz and 5.8 GHz for this

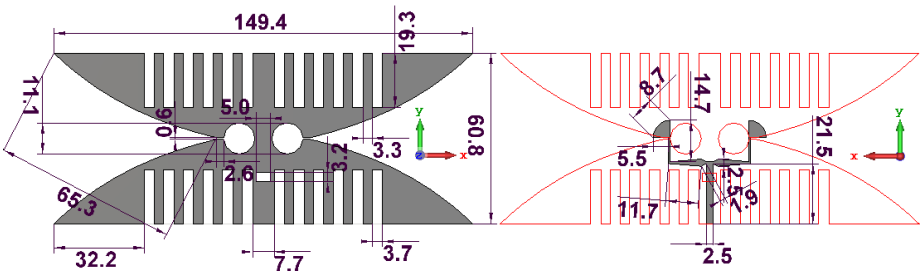

Figure 5: The dimensions of the dual-band back-to-back Vivaldi antennas operating at 2.45 GHz and 5.8 GHz (the dimensions are given in mm)

scenario are given in Fig. 7. At 2.45 GHz, whether the slot line is filled with gallium or not, the beam switching feature is exhibited. However, at 5.8 GHz, the main lobe directions are oriented in the antithetical direction to the prescribed directions, leading to a highly inadequate suppression of back lobes. To surmount this issue, as depicted in Fig. 6-(b), the interior of the slot line is filled with gallium, and the same simulations are re-executed. In this configuration, both the intended radiation direction and a satisfactory decrease in the back lobe level are achieved at 5.8 GHz. Due to the necessity of giving LM a specific shape, the fluidic line in the single-band case was eliminated, and displacement was achieved with a syringe.

3.2 Results of the LM-Assisted Dual-Band Vivaldi Antennas

A transmitter antenna (Tx) and a receiver antenna (Rx) were produced for use in Doppler radar, and fundamental measurements were performed. According to both measurement and simulation results, the antennas have a sufficiently low reflection coefficient at both frequencies for both pattern states; see Fig. 8. Photographs of the ground surface of Rx when the antenna is on State-2 is provided at the bottom of the same figure. In this photo, the holders to be utilized to prevent gallium from flowing out are mounted on the antenna. The maximum gain in the simulation at 2.45 GHz is 5.83 dBi, and the measured realized gain values of Tx and Rx are 5 and 5.2 dBi, respectively. At 5.8 GHz, the simulated realized gain, measured realized gain of Tx and that of Rx are found 7.43, 6.7 and 6.9 dBi, respectively. The simulated FBR at 2.45 GHz is 15 dB for both states, thanks to symmetry. In the measurement, the fact that the maximum FBR values are $\sim$ 12 dB for State-1 of Tx, $\sim$ 11 dB for State-2 of Tx, $\sim$ 12 dB for State-1 of Rx, $\sim$ 13 dB for State-2 of Rx, shows us that the measurements give close results with simulations; see Fig. 9. Although these values are slightly lower at 5.8 GHz, the FBR value for both states of the antennas is above 8 dB in simulation and measurements as shown in Fig. 10, which is sufficient for the selected application.

In Table 1, a comparison with existing pattern reconfigurable antennas in

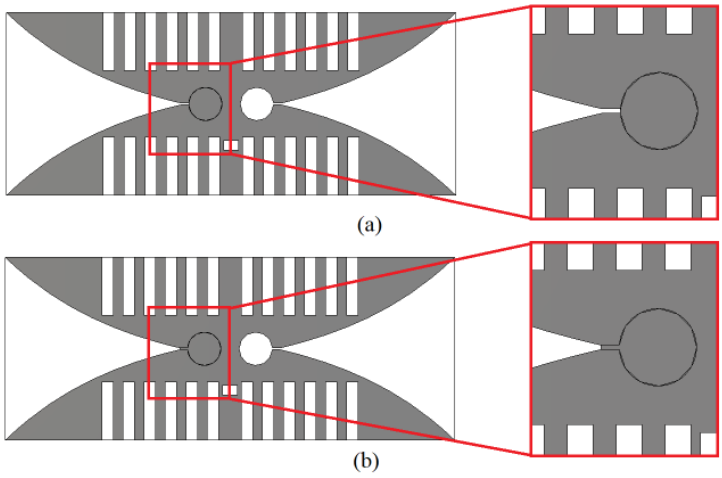

Figure 6: The simulation scenarios carried out to enable beam switching ability at both frequencies of the dual-band LM displacement-enabled Vivaldi antenna (a) State-1 when only the cavity is filled with gallium (b) State-1 when both the cavity and slot line are filled with gallium.

the literature is given. The reconfiguration/switching method and center frequencies are provided at the beginning of the table. The proposed antenna at the lower operating frequency has a smaller electrical size than its counterparts, except for [26]. However, because of the need for an additional bias circuit in [26], the overall size becomes larger than the other structures. Since [27] has a 3-dimensional hexagonal structure, we determined its electrical dimension according to the open form of the hexagon. Two values are given for this study in each of the gain and FBR rows, with the first corresponding to the values at 2.45 GHz, and the second at 5.8 GHz. The primary advantage of the proposed configuration lies in its seamless and cost-effective integration compared to alternatives based on graphene or PIN diodes. Furthermore, its independence from electrical connections eliminates the risk of interference-induced pattern degradation. In contrast to structures relying on PIN diodes with non-continuous transmission lines, the proposed approach boasts greater efficiency due to its uninterrupted surface current. Moreover, while electrical and optical reconfiguration techniques are susceptible to malfunctions and necessitate regular maintenance, the LM displacement-based beam switching method proposed here stands out as a robust, long-term solution.

4 LM-Assisted Power Divider

In this section, a power divider capable of transition between 2.45 GHz and 5.8 GHz through LM displacement is proposed.

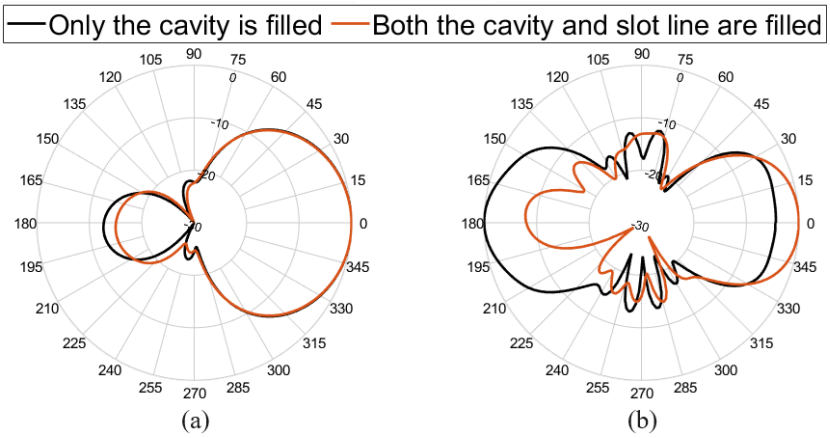

Figure 7: Effect of the slot line on the normalized far-field plot at State-1 when $\theta = 90°$ (a) 2.45 GHz (b) 5.8 GHz

Table 1: Comparison with various pattern reconfigurable antennas

Reference	This work	[25]	[26]	[27]
Shape	Vivaldi	Vivaldi	Arc Dipole	Hexagon
Method	LM	Graphene	PIN Diode	Graphene
Freq. (GHz)	2.45 / 5.8	30	2.7	1500
Size (λ^2)	1.22×0.49	3.2×1.4	0.61×0.61	3×0.44
Gain (dBi)	5.2 / 6.9	3.8	4.1	3.1
FBR (dB)	13 / 9.5	~ 8	~ 8	~ 10
Relative Complexity	Easy	Medium	Medium	Hard
Bias circuit	No	No	Yes	No

4.1 Design of the LM-Assisted Power Divider

A 1:1 T-junction power divider, that can be preferred in various Doppler radar applications [22], with 50 Ω characteristic impedance has been designed using the same material as the antennas. To ensure that the impedance of the divider matches the characteristic impedance of the input line (Z_0 in Fig. 11), the line impedance Z_1 should be 100 Ω. In order to terminate the output ports with 50 Ω impedance, a quarter-wave transformer must be inserted. The impedance of the quarter-wave transformer is approximately $Z_{qw} = \sqrt{Z_1 Z_0} = 70$ Ω. It gives the power divider a frequency selective characteristic, as the length of the transformer should be equal to quarter of the wavelength. One can change the operating frequency of the divider by switching between 2.45 GHz and 5.8 GHz by taking the advantage of this feature in the LM displacement-assisted manner. When the length of the transformer increases, the operating frequency

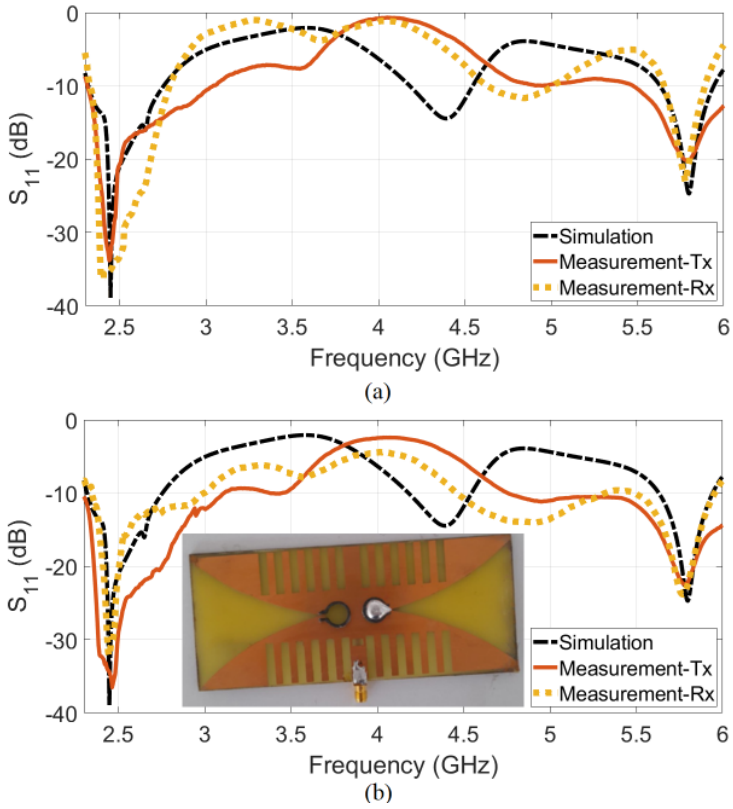

Figure 8: Scattering parameters of the fabricated antennas (a) State-1 (b) State-2

decreases and vice versa. To achieve this goal, two different states, State-A and State-B, have been defined, and the areas to be filled with LM in these states are shown in Fig. 12. If the spaces indicated by the letters A (green regions) and B (orange regions) are filled here, the respective structure is optimized to operate at 2.45 GHz and 5.8 GHz, respectively. When regions A are filled with gallium, the quarter-wave (QW) transformer line corresponds to the effective wavelength of 2.45 GHz, while when regions B are filled with gallium, the same line corresponds to a quarter of the effective wavelength of 5.8 GHz.

4.2 Results of the LM-Assisted Power Divider

After the fabrication of the power divider to be used in the radar, measurements were conducted to assess the reflection and transmission values. To avoid confusion with the antenna states, the power divider states at 2.45 GHz and 5.8 GHz were named State-A and State-B, respectively. As shown in Fig. 13-(a), both simulations and measurements demonstrate that in State-A, around

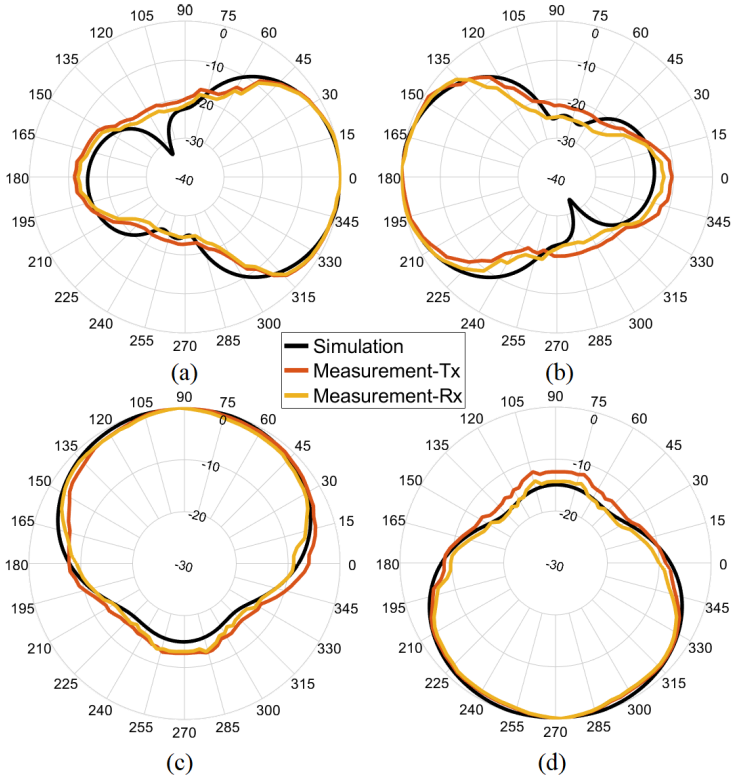

Figure 9: Normalized far-field plots of the dual-band antennas at 2.45 GHz (a) State-1 when $\theta = 90°$ (b) State-2 when $\theta = 90°$ (c) State-1 when $\phi = 0°$ (d) State-2 when $\phi = 0°$

2.45 GHz, the S_{11} value is significantly low. Similarly, in State-B, the same graph reaches its minimum value around 5.8 GHz. This observation clearly indicates the frequency-switching capability of the designed LM-assisted power divider and provides a significant advantage in protecting against potential noise at frequencies other than those at which the radar operates.

In Fig. 13-(b), the power ratios transmitted to the second and third ports are provided. In State-A, the transmission value increases at the frequency of 2.45 GHz, while in State-B, the transmission achieves higher values at the frequency of 5.8 GHz. Observing the green, yellow, and cyan-colored lines, they attain higher values at 5.8 GHz compared to 2.45 GHz. Similarly, the transmission value at 2.45 GHz is higher than the transmission value at 5.8 GHz for the black, blue, and red-colored lines. The agreement between the simulation and measurement further demonstrates the robustness of this methodology. Located at the lower section of this figure, firstly, an unmerged version of the power divider along with its corresponding port numbers is shown. Secondly, it demonstrates the channels through which the power divider in State-B con-

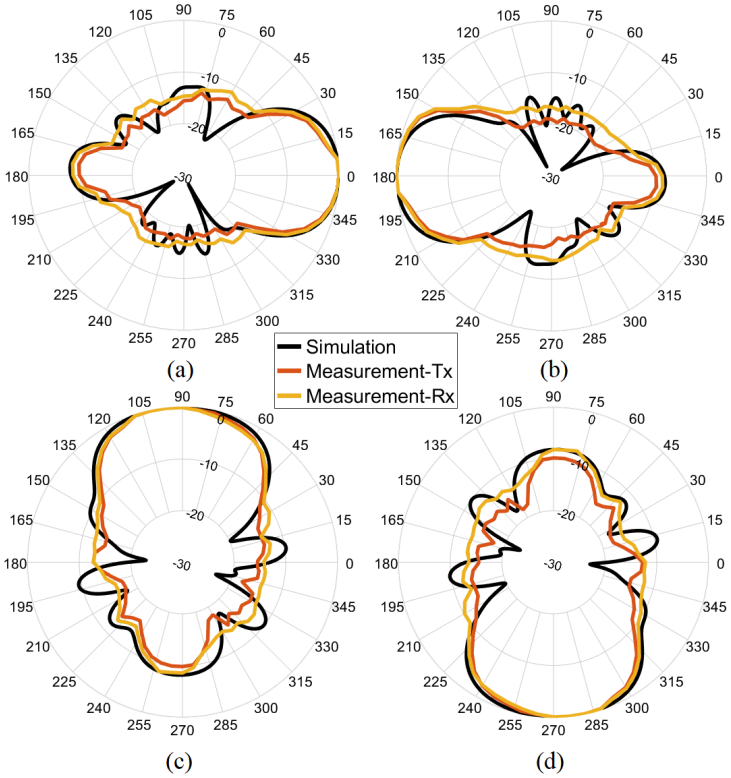

Figure 10: Normalized far-field plots of the dual-band antennas at 5.8 GHz (a) State-1 when $\theta = 90°$ (b) State-2 when $\theta = 90°$ (c) State-1 when $\phi = 0°$ (d) State-2 when $\phi = 0°$

dition. It is noteworthy that polyurethane has been selected as the preferred material for the liquid channel in this particular context.

5 Doppler Radar Results

After the fabrication of the components and equipping them with switchable features, the fabricated structures were integrated into an operating Doppler radar system with CW operation. Fig. 14 presents a simplified block diagram and the photograph of the relevant configuration, where the Rx, Tx, and power divider structures have been reconfigured with LM. In this configuration, the frequency of the input signal can be adjusted through the voltage-controlled oscillator. By enabling the power divider to switch between State-A and State-B, radar operation at either 2.45 GHz or 5.8 GHz can be achieved in this setup. In each state, velocity measurements were obtained. Based on Fig. 14-(a), when the antennas are in State-1, the radar perceives the direction on the right

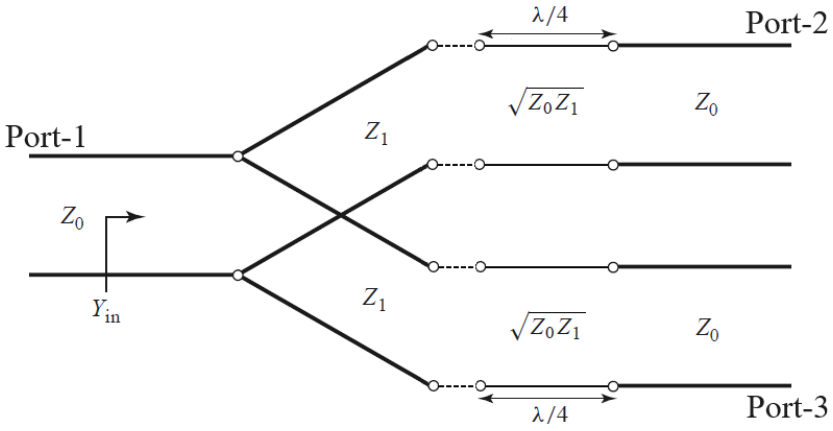

Figure 11: Transmission line equivalent of the power divider

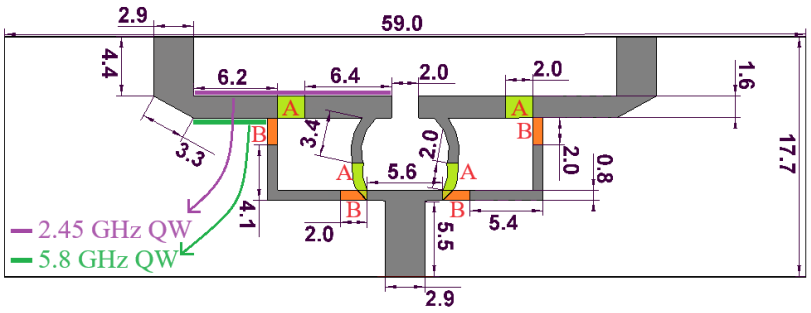

Figure 12: Dimensions of the LM displacement-enabled power divider (the dimensions are given in mm)

side. Conversely, when the antennas transition to State-2, the radar detects the direction on the left side. A photograph depicting the syringe-assisted state change of the antenna, as well as the integrated versions of the antennas into the radar, can be observed in Fig. 15.

In Fig. 16, depicting a particular measurement scenario, the target undergoes continuous movement at the illustrated position while the antenna states are altered using a syringe. Similar movements were executed at approximately the same locations for each measurement scenario, and the measurements were completed. A moving person initiated motion at a distant point from the radar, accelerated towards it, and gradually decelerated as it approached. Upon reaching the radar, the person briefly waited before moving away with a similar pattern of acceleration and deceleration. We want to emphasize here that the moving person performs the same movements at approximately the same velocities in all four measurement setups. However, as can be seen in Fig. 16-(a) and Fig. 16-(c), when the antennas are in State-1, the moving person is detected by

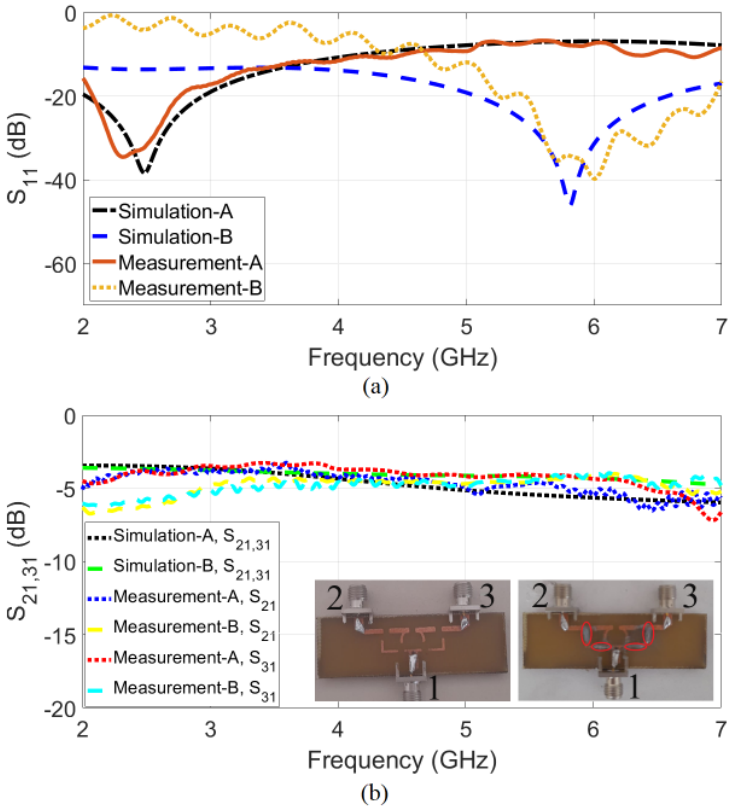

Figure 13: Scattering parameters of the power divider (a) S_{11} (b) S_{21} and S_{31}. The manufactured power divider, along with port numbers and the photographs of the polyurethane channels, are also provided.

the radar because it falls within the radar's footprint. On the other hand, when the antennas are in State-2, the direction of observation by the radar rotates by 180 degrees. As a result, no movement signal related to the target of interest is detected, exactly as intended. In scenarios where the frequencies of radar states periodically change, it becomes possible to distinguish between two moving objects located within the radar's range but in separate sectors. In other words, in the presence of multiple moving objects, the radar can differentiate the velocity of these two objects through this configuration. Additionally, through frequency switching, the radar aims to seamlessly continue its operation by switching to another frequency band in the case of a potential interference threat to the currently used band.

In Fig. 17-(a) and 17-(c), the antennas are in State-1, and a pendulum with an aluminum ball is in the radar's footprint at the right side and a moving person approaching the radar at the left side according to the Fig. 14. Due to the pendulum being metallic and causing Doppler shifts at multiple frequencies si-

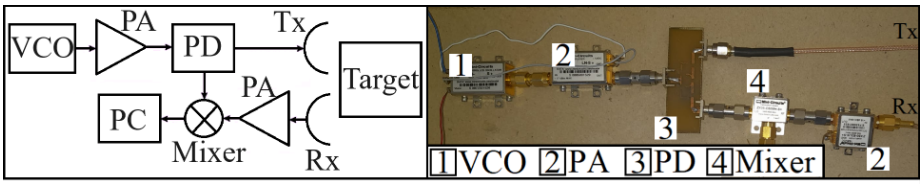

Figure 14: A simplified block diagram and the photograph of the radar configuration. (VCO: Voltage-controlled oscillator, PD: Power Divider, PA: Power Amplifier, PC: Personal Computer.) (a) Scheme (b) Photograph

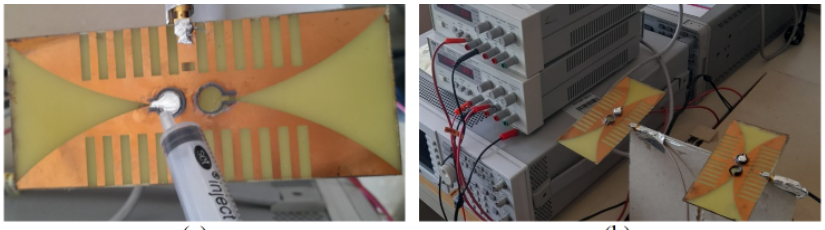

Figure 15: Photos of the proposed structures (a) Reconfiguration of the Vivaldi antenna by means of LM displacement (b) Antennas with LM connected to the radar system

multaneously, no noticeable noise arising from the moving person was observed in this state. When considering the use of an approximately 1-meter long string, it can be concluded that from the conversions of potential energy and kinetic energy, the velocity of the ball is accurately measured at both frequencies. The maximum velocity of the pendulum, hanging from a one-meter string, was measured at approximately 4 m/s in the first swing for both states. This velocity decreased in accordance with the pendulum equation. On the other hand, in Fig. 17-(b) and 17-(d), the radar beam is oriented towards a direction where the moving person is present. Thus, the velocity of the moving person approaching the radar could be measured, but due to finite FBR values, movements of the pendulum remaining in the backlobe, even at a low power level, were observed as the noise in these measurements. Adjusting the dynamic range to a level lower than 35 dB, at the expense of filtering out some parts of the primary movement, can help eliminate this noise. As the FBR is lower at 5.8 GHz compared to 2.45 GHz, this backward detection is slightly more pronounced in the 5.8 GHz measurements.

Table 2 compares the performance of the proposed radar compared to various studies based on MIT-CCDR in the literature. Numerous studies have been conducted in the literature to develop and enhance the operational capability of MIT-CCDR over time. While the literature commonly presents this radar as a single-band configuration, this configuration has been transformed into a

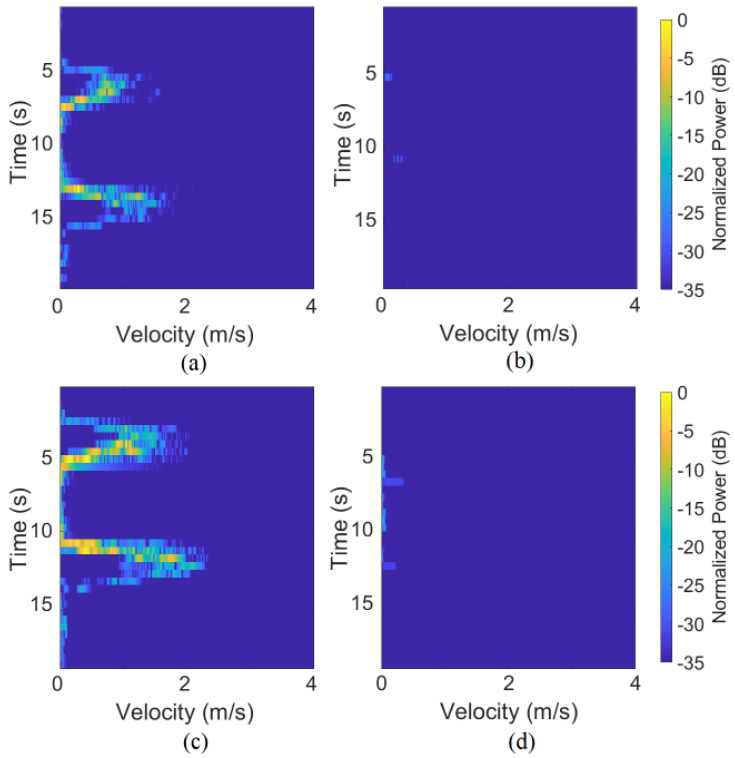

Figure 16: Velocity measurement of a walking person when the radar is at (a) State-A-1 (b) State-A-2 (c) State-B-1 (d) State-B-2

dual-band capable system with the proposed design. Additionally, for the first time in the literature, the structure has been endowed with frequency switching capability through LM displacement, ensuring noise immunity. This configuration, which solely relies on microstrip antenna structures, is lighter than its counterparts. Moreover, in the literature, there have been previous studies that endowed this configuration with beam-steering capability. However, as far as our knowledge extends, this process has been realized for the first time in this study through the LM-assisted technique, thus eliminating the disadvantages of the conventional methods when detecting multiple moving objects.

6 Conclusions

This paper addresses longstanding challenges associated with conventional electrical, optical and physical alteration-based reconfiguration methods to enhance multiple parameters of an operational Doppler radar system by means of novel techniques. The proposed beam switching method has been demonstrated on a single-band back-to-back Vivaldi antenna, followed by its upgrade to a dual-

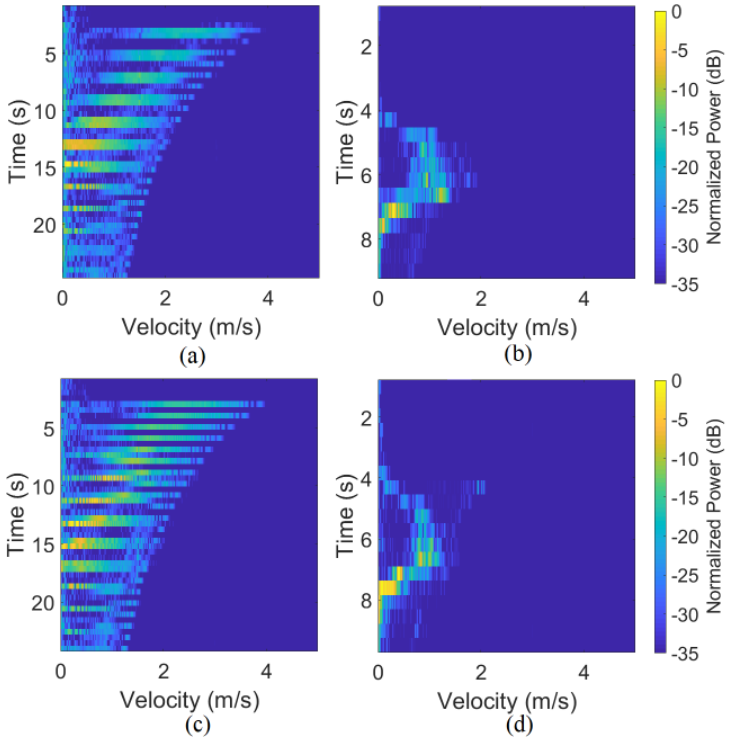

Figure 17: Velocity measurement of a pendulum when the radar is at (a) State-A-1 (b) State-A-2 (c) State-B-1 (d) State-B-2

band configuration, thereby ensuring the usability of the same feature in both frequency bands. Through a slight shift in the position of the LM, one can revert the radar's viewing angle by 180 degrees. Given PIN diodes' discrete nature, this achievement would have presented significant difficulties if attempted with electrical methods, underscoring the advantage of LM's continuous structure in improving radiation efficiency. Additionally, the integration of the LM-controlled novel power divider for frequency switching enhances the practicality and robustness of the radar system. The proposed method enables real-time adjustments to Doppler radar parameters by modifying the antenna's main lobe direction and the divider's operating frequency without any electrical and optical attachments. While, for the purpose of demonstrating the effectiveness of the method, the manual dripping method was employed in this study, the automation of this structure through the use of liquid pumps can be realized in future studies. Automating the proposed technique using diverse pumps in the future poses an engineering challenge that requires careful consideration to prevent any oscillation or disturbance in the antenna and other components during the measurements. The devised system has demonstrated its capability to accurately measure the velocities of moving entities such as walking per-

Table 2: Comparison of various MIT-CCDR-based CW radars (MS: Microstrip, CC: Coffee Can, MM: Metamaterial)

Reference	This work	[21]	[22]	[28]
Freq. (GHz)	2.45 / 5.8	2.4	2.45	5.8
Antenna type	MS	CC	MS	MS+MM
Footprint (deg.)	120 / 60	75	35	60
Beam-steering	Liquid	No	Mechanical	No
Freq. Switching	Yes	No	No	No
Noise immunity	High	Low	Moderate	Moderate
Multi-target	Yes	No	Yes	No

son and pendulum, within both frequency bands. Furthermore, it has shown suitability for multi-target detection by effectively eliminating obstructed sector movements.

References

[1] D. Tang, J. Wang, W. Hu, Z. Peng, Y.-C. Chiang, and C. Li, "A dc-coupled high dynamic range biomedical radar sensor with fast-settling analog dc offset cancelation," *IEEE Transactions on Instrumentation and Measurement*, vol. 68, no. 5, pp. 1441–1450, 2019.

[2] S. Prager, T. Thrivikraman, M. S. Haynes, J. Stang, D. Hawkins, and M. Moghaddam, "Ultrawideband synthesis for high-range-resolution software-defined radar," *IEEE Transactions on Instrumentation and Measurement*, vol. 69, no. 6, pp. 3789–3803, 2019.

[3] E. Motovilova and S. Y. Huang, "A review on reconfigurable liquid dielectric antennas," *Materials*, vol. 13, pp. 1–28, 2020.

[4] X. Xu, P. Xu, Y. Wang, Z. Wang, K. Yu, H. Shi, D. Ge, X. Ma, G. Leng, M. Wang *et al.*, "Intelligent design of reconfigurable microstrip antenna based on adaptive immune annealing algorithm," *IEEE Transactions on Instrumentation and Measurement*, vol. 71, pp. 1–14, 2022.

[5] A. Raza, R. Keshavarz, E. Dutkiewicz, and N. Shariati, "Compact multi-service antenna for sensing and communication using reconfigurable complementary spiral resonator," *IEEE Transactions on Instrumentation and Measurement*, vol. 72, pp. 1–9, 2023.

[6] C. G. Christodoulou, Y. Tawk, S. A. Lane, and S. R. Erwin, "Reconfigurable antennas for wireless and space applications," *Proceedings of the IEEE*, vol. 100, no. 7, pp. 2250–2261, 2012.

[7] P. B. Nikam, J. Kumar, V. Sivanagaraju, and A. Baidya, "Dual-band reconfigurable ebg loaded circular patch mimo antenna using defected ground

structure (dgs) and pin diode integrated branch-lines (bls)," *Measurement*, vol. 195, p. 111127, 2022.

[8] N. Ojaroudi Parchin, H. Jahanbakhsh Basherlou, Y. I. Al-Yasir, A. M. Abdulkhaleq, and R. A. Abd-Alhameed, "Reconfigurable antennas: Switching techniques—a survey," *Electronics*, vol. 9, no. 2, p. 336, 2020.

[9] V. T. Bharambe, J. Ma, M. D. Dickey, and J. J. Adams, "Reshape: A liquid metal-based reshapable aperture for compound frequency, pattern, and polarization reconfiguration," *IEEE Transactions on Antennas and Propagation*, vol. 69, no. 5, pp. 2581–2594, 2020.

[10] V. Bharambe, D. P. Parekh, C. Ladd, K. Moussa, M. D. Dickey, and J. J. Adams, "Liquid-metal-filled 3-d antenna array structure with an integrated feeding network," *IEEE Antennas and Wireless Propagation Letters*, vol. 17, no. 5, pp. 739–742, 2018.

[11] G. J. Hayes, J.-H. So, A. Qusba, M. D. Dickey, and G. Lazzi, "Flexible liquid metal alloy (egain) microstrip patch antenna," *IEEE Transactions on Antennas and Propagation*, vol. 60, no. 5, pp. 2151–2156, 2012.

[12] A. Ha, M. H. Chae, and K. Kim, "Beamwidth control of an impulse radiating antenna using a liquid metal reflector," *IEEE Antennas and Wireless Propagation Letters*, vol. 18, no. 4, pp. 571–575, 2019.

[13] X. Yang, Y. Liu, H. Lei, Y. Jia, P. Zhu, and Z. Zhou, "A radiation pattern reconfigurable fabry–pérot antenna based on liquid metal," *IEEE Transactions on Antennas and Propagation*, vol. 68, no. 11, pp. 7658–7663, 2020.

[14] J. Hao, J. Ren, X. Du, J. H. Mikkelsen, M. Shen, and Y. Z. Yin, "Pattern-reconfigurable yagi-uda antenna based on liquid metal," *IEEE Antennas and Wireless Propagation Letters*, vol. 20, no. 4, pp. 587–591, 2021.

[15] Z. Chen, H. Wong, and J. Kelly, "A polarization-reconfigurable glass dielectric resonator antenna using liquid metal," *IEEE Transactions on Antennas and Propagation*, vol. 67, no. 5, pp. 3427–3432, 2019.

[16] G. B. Zhang, R. C. Gough, M. R. Moorefield, K. J. Cho, A. T. Ohta, and W. A. Shiroma, "A liquid-metal polarization-pattern-reconfigurable dipole antenna," *IEEE Antennas and Wireless Propagation Letters*, vol. 17, no. 1, pp. 50–53, 2018.

[17] L. Song, W. Gao, C. O. Chui, and Y. Rahmat-Samii, "Wideband frequency reconfigurable patch antenna with switchable slots based on liquid metal and 3-d printed microfluidics," *IEEE Transactions on Antennas and Propagation*, vol. 67, no. 5, pp. 2886–2895, 2019.

[18] A. Karatay, "A symmetrical self-diplexing microstrip antenna with eight-shaped defects," *Journal of Electromagnetic Waves and Applications*, vol. 36, no. 16, pp. 2305–2319, 2022.

[19] K. Y. Alqurashi, J. R. Kelly, Z. Wang, C. Crean, R. Mittra, M. Khalily, and Y. Gao, "Liquid metal bandwidth-reconfigurable antenna," *IEEE Antennas and Wireless Propagation Letters*, vol. 19, no. 1, pp. 218–222, 2020.

[20] J. Carroll, G. Paparisto, and D. Vye, "The "coffee-can" radar redesigned as an inexpensive RF PCB [application notes]," *IEEE Microwave Magazine*, vol. 17, no. 10, pp. 62–74, 2016.

[21] G. L. Charvat, A. J. Fenn, and B. T. Perry, "The MIT IAP radar course: Build a small radar system capable of sensing range, Doppler, and synthetic aperture (SAR) imaging," in *2012 IEEE Radar Conference*. IEEE, 2012, pp. 0138–0144.

[22] A. Karatay, D. Orcan, C. Özkal, and F. Yaman, "Implementation and experimental verifications of microstrip antennas for angular scanning of a Doppler radar," *AEU-International Journal of Electronics and Communications*, vol. 101, pp. 76–84, 2019.

[23] J.-M. Munoz-Ferreras, Z. Peng, Y. Tang, R. Gomez-Garcia, D. Liang, and C. Li, "Short-range doppler-radar signatures from industrial wind turbines: Theory, simulations, and measurements," *IEEE Transactions on Instrumentation and Measurement*, vol. 65, no. 9, pp. 2108–2119, 2016.

[24] A. A. Pramudita and F. Y. Suratman, "Low-power radar system for non-contact human respiration sensor," *IEEE Transactions on Instrumentation and Measurement*, vol. 70, pp. 1–15, 2021.

[25] C. Fan, B. Wu, Y. Hu, Y. Zhao, and T. Su, "Millimeter-wave pattern reconfigurable vivaldi antenna using tunable resistor based on graphene," *IEEE Transactions on Antennas and Propagation*, vol. 68, no. 6, pp. 4939–4943, 2019.

[26] G. Jin, M. Li, D. Liu, and G. Zeng, "A simple planar pattern-reconfigurable antenna based on arc dipoles," *IEEE Antennas and Wireless Propagation Letters*, vol. 17, no. 9, pp. 1664–1668, 2018.

[27] B. Wu, Y. Hu, Y. T. Zhao, W. B. Lu, and W. Zhang, "Large angle beam steering THz antenna using active frequency selective surface based on hybrid graphene-gold structure," *Optics Express*, vol. 26, no. 12, pp. 15 353–15 361, 2018.

[28] H. Ö. Yılmaz and F. Yaman, "Metamaterial antenna designs for a 5.8-ghz doppler radar," *IEEE Transactions on Instrumentation and Measurement*, vol. 69, no. 4, pp. 1775–1782, 2019.